

FIRST-ORDER PERTURBATION APPROACH TO TRANSFORMER WINDING DEFORMATIONS

Mariana Dalarsson* and Martin Norgren

Department of Electromagnetic Engineering, School of Electrical Engineering, KTH Royal Institute of Technology, Stockholm SE-100 44, Sweden

Abstract—An on-line method to detect radial mechanical deformations of power transformer winding turns is presented. First-order perturbation theory is applied to a transformer winding surrounded by the transformer tank wall and the iron core. The transformer winding is modeled as thin conducting cylindrical rings (winding segments or turns) situated within a coaxial waveguide, where the outer conducting cylinder represents the transformer tank wall while the inner conducting cylinder represents the iron core. Antennas which radiate and measure microwave fields are proposed inside the transformer tank in order to identify and quantify the mechanical deformations of winding turns. The direct propagation problem is solved using conventional waveguide theory with mode-matching and cascading techniques. An optimization algorithm is then used to solve the inverse problem whereby a good agreement between the reconstructed and true deformations of the winding segments is obtained.

1. INTRODUCTION

A power transformer is one of the most critical components in the electric power grid, the occasional failure of which may result in major consequences for the power supply ability of the grid. Power transformers are subject to several degradation mechanisms during operation, including thermal degradation at hot spots, partial discharges due to local electric field surges, winding deformations caused by mechanical forces from short circuit currents, and increased levels of moisture in the cellulose insulation due to decomposition.

Received 23 July 2013, Accepted 7 September 2013, Scheduled 10 September 2013

* Corresponding author: Mariana Dalarsson (mardal@kth.se).

The abovementioned degradation phenomena can be detected using the available diagnostic methods. However, the available diagnostic methods are often inaccurate or only applicable off-line. Off-line methods generally imply a non-service stress of a transformer.

Some proposed on-line methods are presented in [1–4]. For a brief survey of these methods, see e.g., Section 2 in [3], where, e.g., the methods of dissolved gas analysis, in-service partial discharge test (PD), short-circuit reactance measurements, FRA frequency response tests and measurements of the vibration intensity of the transformer tank, are described. From the descriptions in [3] and elsewhere, it is reasonable to conclude that neither of these methods is capable to detect and quantitatively measure the actual individual deformations of the winding segments or turns. The reason for that being that the results of their measurements are generally only indirectly related to the individual conductor deformations. It is therefore fair to say that, as far as the detection of the individual winding conductor deformations is concerned, the accuracy of the available on-line methods is limited.

Thus, as far as the present authors are aware of, on-line monitoring methods of individual winding deformations due to the mechanical forces from short circuit currents and/or initial manufacturing inconsistencies are generally not available. In this paper, we therefore study a principle for an on-line method, which is capable to detect and measure the individual mechanical deformations, where one or more winding turns have been slightly deformed from the ideal circular form to either a simple elliptic form or more realistic wave-shaped form, described in detail below. Our general method [5,6] can in principle also be used to detect the effects of other types of degradation mechanisms (see e.g., [7]), but the investigation in the present paper focuses on a specific class of mechanical deformations only.

The present approach is based on inserting antennas inside the transformer tank, above and below the transformer windings, which radiate and measure microwave fields. The microwave fields interact with the winding structure, and the analysis of the measured signals and their relations to the mechanical structure parameters, which are critical signatures of mechanical deformations, is an inverse electromagnetic problem [8]. In this paper, the direct propagation problem is solved by means of the conventional waveguide theory, including mode-matching and cascading techniques [9], while the inverse problem is solved using an optimization technique which allows us to reconstruct the deformations of the irradiated winding turns.

In the present paper, we use similar methods for solving both the direct and inverse problems as in [5,6], and in that sense the

present investigation is incremental as compared to our previous work [5,6]. It should, however, be noted that the present paper is not directly concerned with the conductor displacement problems described in [5,6]. The objective of the present paper is the study of the elliptic, and more importantly, the wave shaped mechanical deformations of transformer windings only. This type of deformations is more realistic and more often encountered in actual decommissioned power transformers compared to the deformations studied in [5,6], such that any realistic future diagnostic device will need the mathematical tools to describe the wave-shaped deformations. As far as the present authors are aware, the study of such mathematical tools, using perturbation techniques, is not found in the literature.

Furthermore, we would like to add that this paper provides a proof that the wave-shaped deformations (to the first-order approximation) can be reduced to the simple displacements reported in [5,6] with the suitable choice of the TM-modes, being an important new result showing that essentially the same mathematical tools can be used to cover the broad range of deformations. It is an important step towards any realistic design of a diagnostic device.

2. THE UNPERTURBED PROBLEM DESCRIPTION

We model a transformer winding structure as a coaxial cylindrical waveguide, where the outer conducting cylinder represents the transformer tank wall while the inner conducting cylinder represents the iron core [6], as shown in Fig. 1. Between the transformer tank wall and the iron core there is a set of thin conducting cylindrical

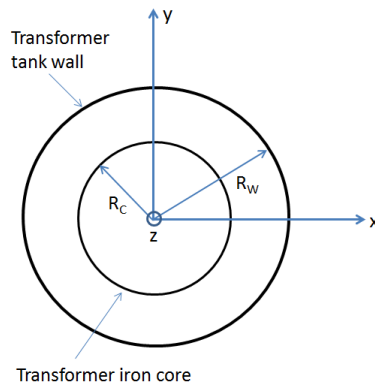


Figure 1. The power transformer as a coaxial cylindrical waveguide.

rings (winding turns) that are situated within the coaxial cylindrical waveguide. The geometry of our model of a transformer winding surrounded by the transformer-tank wall and the iron core is shown in Fig. 2. We denote the four regions (1–4) between the two cylindrical conductive surfaces of the coaxial waveguide (iron core and tank wall) and the conductive obstacle (winding turn) as indicated in Fig. 2.

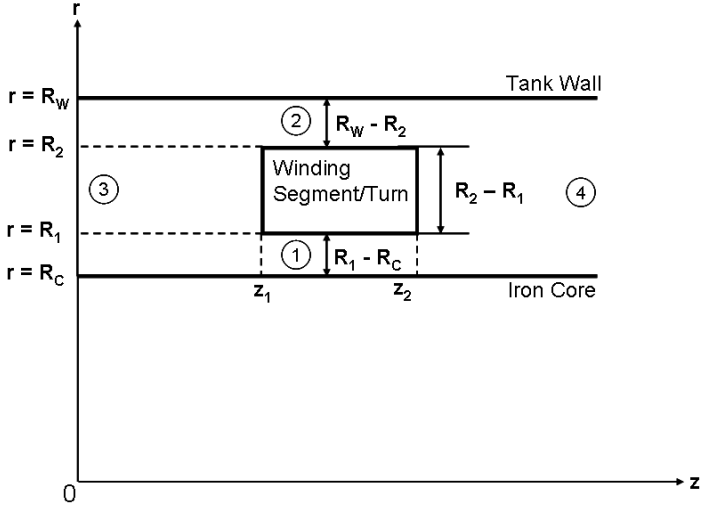


Figure 2. Cross section of a coaxial waveguide as a model of a transformer winding.

For the propagation problem we only consider TM-modes ($H_z = 0$) as they include the TEM-mode, which is the dominant mode in all regions. Following [11], the longitudinal component of the electric field is given by

$$E_z = \frac{1}{\sigma + j\omega\epsilon} \left(\frac{d^2\Lambda}{dz^2} + k^2\Lambda \right) T(r, \varphi), \quad (1)$$

where $k^2 = j\omega\mu(\sigma + j\omega\epsilon)$ and $\Lambda(z) = \exp(-jk_z z)$ for waves propagating in the positive z -direction. The material parameters μ , σ and ϵ are the effective permeability, conductivity and permittivity, respectively, for the transformer winding insulation. The scalar transverse function denoted by $T(r, \varphi)$ in (1) for TM-waves in a coaxial wave guide is a solution of the transverse wave equation

$$\nabla_T T(r, \varphi) + \gamma^2 T(r, \varphi) = 0, \quad (2)$$

where γ is the transverse wave number. An approximate solution of the

Equation (2) for TM-waves, suitable for our problem, is given by [11]

$$T_{n,m}(r, \varphi) = Q \sin \frac{n\pi(r - R_I)}{R_O - R_I} \cos(m\varphi), \quad (3)$$

with

$$\gamma_{n,m}^2 = \frac{n^2\pi^2}{(R_O - R_I)^2} + \frac{4m^2}{(R_I + R_O)^2}, \quad (4)$$

where $n = 1, 2, \dots$ and $m = 0, 1, 2, \dots$ are two integers that denote the TM-modes in this case. In (3) and (4) we denote the radii of the inner and outer cylinders of the coaxial waveguide cavity by R_I and R_O respectively.

3. MECHANICAL DEFORMATIONS IN POLAR COORDINATES

Let us first assume that the transformer winding turn of radius R (equal to inner radius R_1 or outer radius R_2 , according to Fig. 2 for regions 1 and 2, respectively) lying between the iron core of radius R_C and the transformer tank of radius R_W , is slightly deformed from the expected circular shape of radius R to an ellipse with semi-major axis a and semi-minor axis b . The ideal circular shape and the actual deformed elliptic shape of the transformer winding turn are shown in Fig. 3(a).

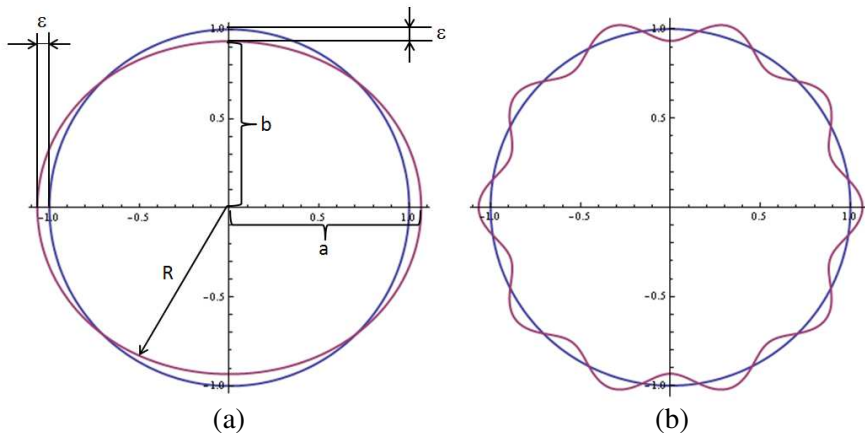


Figure 3. Mechanical deformations of a circular winding of radius R . (a) Simple elliptic deformation and (b) more realistic wave-shaped deformation.

From Fig. 3(a), to the first order of approximation in the small parameter ε/R , we obtain the following result for the size of the radial deformation $\delta(r, \varphi)$ of the elliptic winding compared to the unperturbed circular winding

$$\delta(r, \varphi) = \delta(\varphi) = r - R = \varepsilon \cos(2\varphi). \quad (5)$$

From (5), we see that $a - R = +\varepsilon$ for the semi-major axis ($r = a$) when $\varphi = 0, \pi$, while $b - R = -\varepsilon$ for the semi-minor axis ($r = b$) when $\varphi = \pi/2, 3\pi/2$ in accordance with Fig. 3(a). Thus we have $a = R + \varepsilon$ and $b = R - \varepsilon$ such that, to the second order of approximation in the small parameter ε/R , the length of the perturbed ellipse is given by

$$O = 2\pi R \left(1 + \frac{\varepsilon^2}{4R^2} \right) \approx 2\pi R, \quad (6)$$

and we see that up to the first order in the small parameter ε/R , the turn length of the winding is unaffected by the perturbation.

Although possible in principle, the simple elliptic deformation as the one depicted in Fig. 3(a) is unlikely in realistic power transformer windings. The reason for that observation is that the power transformer windings are wound in such a way that their circumference is partly mechanically supported by a number of solid state (pressboard) spacers, distributed periodically over the winding circumference. In between these spacers there are vertical oil ducts, where the transformer oil can flow in order to reduce the temperature gradient between winding conductors and surrounding oil, such that the hot spot temperature is kept to a minimum. This reduces the rate of degradation of the winding insulation due to hot spots and consequently ensures a longer life expectancy of a power transformer [12].

However, when subject to heavy radial forces due to short circuit currents, the parts of the circumference of the winding turns, less supported by the solid state insulation, are more likely to be deformed towards the iron core than the parts fully supported by the solid state insulation [12]. Such deviations are indeed sometimes found when inspecting old decommissioned power transformers. Some typical mechanical deformations of winding turns are shown and studied using frequency response analysis (FRA) in, e.g., [13]. Thus, a realistic winding deformation can be modeled by a wave-shaped form depicted in Fig. 3(b), where we have chosen (as an example) that there are exactly ten segments supported by the solid state insulation and consequently another ten segments between them that are less supported by solid state insulation. Thus, the cross section of a winding segment, seen from the above, displays a periodic wave-shape as shown in Fig. 3(b).

Analogously to the case of the elliptic deformation above, to the first order of approximation in the small parameter ε/R , we obtain the following result for the size of the radial deformation $\delta(r, \varphi)$ of the wave-shaped deformed winding compared to the unperturbed circular winding

$$\delta(r, \varphi) = \delta(\varphi) = r - R = \varepsilon \cos(10\varphi). \quad (7)$$

The result (7) is of course valid for the actual example depicted in Fig. 3(b), where there are exactly ten segments supported by the solid state insulation. In general, if the winding manufacturing technology stipulates some other number k of supporting segments, the general result analogous to (7) reads

$$\delta(r, \varphi) = \delta(\varphi) = r - R = \varepsilon \cos(k\varphi). \quad (8)$$

In the present paper, we will use the example with $k = 10$ to derive the general results, but all the results and conclusions throughout the paper have a general validity, and can be derived without reference to this particular example in a straightforward way.

4. THE FIRST-ORDER PERTURBATION MODEL

Following [10] (Problem 8.12), if the eigenvalue parameters and eigenfunctions of the transverse equation for two boundary contours C and C_0 are (γ^2, T) and (γ_0^2, T_0) , respectively, then to the first order in $\delta(r, \varphi)$ we have for TM-modes

$$\gamma^2 - \gamma_0^2 = - \frac{\oint_{C_0} \delta(\varphi) \left| \frac{\partial T_0}{\partial n} \right|^2 dl_0}{\int_{S_0} |T_0(r, \varphi)|^2 dS_0}, \quad (9)$$

where $\partial T / \partial n = \mathbf{n} \cdot \nabla T$ is the derivative in the direction of the surface normal. In our case, the unperturbed transverse mode functions for TM-modes are given by (3). Performing the integrations in (9) for the case of a simple elliptic deformation depicted in Fig. 3(a), we obtain

$$\gamma^2 - \gamma_0^2 = \frac{n^2 \pi^2}{(R_O - R_I)^2} \frac{\varepsilon}{R_O - R_I} \delta_{n,1}, \quad (10)$$

where $\delta_{n,1}$ is the Kronecker delta function and should not be confused with our deformation parameter $\delta(r, \varphi)$ or $\delta(\varphi)$. On the other hand, performing the integrations in (9) for the case of a more realistic deformation depicted in Fig. 3(b) with $k = 10$, we obtain

$$\gamma^2 - \gamma_0^2 = \frac{n^2 \pi^2}{(R_O - R_I)^2} \frac{\varepsilon}{R_O - R_I} \delta_{n,5}, \quad (11)$$

From the result (11), we observe an interesting property of the first-order perturbation formula (9) that for any even number $k = 2, 4, 6, \dots$, we obtain the general result

$$\gamma^2 - \gamma_0^2 = \frac{n^2 \pi^2}{(R_O - R_I)^2} \frac{\varepsilon}{R_O - R_I} \delta_{n,k/2}, \quad (12)$$

where we again note that $\delta_{n,k/2}$ is a Cronecker delta function and should not be confused with our deformation parameter $\delta(r, \varphi)$ or $\delta(\varphi)$.

Thus we see that, to the first order of perturbation, only the TM-modes with $m = k/2$, i.e., TM $_{m,k/2}$ -modes, give a non-zero deviation of the eigenvalues γ^2 from the unperturbation eigenvalue parameters γ_0^2 . This property of the first-order perturbation model, described by the result (12), indicates the possibility to distinguish between the different types of mechanical deformations that can occur in a transformer winding structure. If there is a genuine radial deformation of the winding turns described in [6], it will be detected by the lowest TM-mode of microwave radiation with $n = 0$ and the contributions from the higher-order modes will be very small compared to the leading TM $_{m,0}$ -mode.

On the other hand, if we have an elliptic deformation as the one depicted in Fig. 3(a), then it will only be detected by the TM-mode of microwave radiation with $n = 1$ and the contributions from all the other modes ($n = 0$ and $n > 1$) will be small compared to the leading TM $_{m,1}$ -mode. Finally, if there is a wave-shaped deformation as the one depicted in Fig. 3(b), and we know from the winding design specifications that there is an even number k of solid state insulation spacers around the winding circumference, then such a deformation will be detected by the TM-mode of microwave radiation with $n = k/2$ and the contributions from all the other modes ($n < k/2$ and $n > k/2$) will be small compared to the leading TM $_{m,k/2}$ -mode.

There is therefore a clear distinction between the displacements results presented in [5,6], which were obtained using the leading TM $_{m,0}$ -mode, and the wave-shaped deformation results presented here. The wave-shaped deformations are, to the first order of approximation, undetectable by the leading TM $_{m,0}$ -mode and in the results presented in the present paper the leading mode is effectively excluded. Only the TM $_{m,k/2}$ -mode is used when performing the calculations in the present investigation. In particular, the numerical results are obtained with TM $_{m,5}$ -mode.

Thus, in the first-order approximation, by switching on and off microwave antennas with different frequency modes of TM-waves it is, at least in principle, possible not only to detect the radial deformations, but also to determine their general shape. Using now the result (4)

with $m = k/2$, we obtain the perturbed eigenvalue parameters γ^2 in the form

$$\gamma_{n,k/2}^2 = \frac{n^2\pi^2}{(R_O - R_I)^2} \left(1 + \frac{\varepsilon}{R_O - R_I} \right) + \frac{4}{(R_O + R_I)^2}. \quad (13)$$

Thus, in the regions 1 and 2, as depicted in Fig. 2, the mechanical deformation is equivalent to an effective decrease of R_1 and R_2 , i.e.,

$$R'_1 = R_1 - \frac{\varepsilon}{2}, \quad R'_2 = R_2 - \frac{\varepsilon}{2}. \quad (14)$$

On the other hand, the radii of the iron core and the tank wall are clearly not affected by the wave-shaped deformation of the winding turns. Thus in the regions 3 and 4, as depicted in Fig. 2, there are no effects of the wave-shaped perturbation and we can use the unperturbed eigenfunctions and eigenvalue parameters. We can therefore introduce a new variable $\rho = r - R_C$ and replace the mode numbers $(n, k/2)$ simply by (n) . Following [6], we define the orthonormal basis functions for TM_n -modes ($TM_{m,k/2}$ -modes) in the regions 1 (below the conductive obstacle) and 2 (above the conductive obstacle) as follows

$$\psi_n^{(1)}(\rho, \varphi) = \sqrt{\frac{2 - \delta_{n,0}}{\pi(R'_1 - R_C)}} \cos\left(\frac{n\pi\rho}{(R'_1 - R_C)}\right) \cos\left(\frac{k}{2}\varphi\right), \quad (15)$$

$$\psi_n^{(2)}(\rho, \varphi) = \sqrt{\frac{2 - \delta_{n,0}}{\pi(R_W - R'_2)}} \cos\left[\frac{n\pi}{\pi(R_W - R'_2)}(a - \rho)\right] \cos\left(\frac{k}{2}\varphi\right), \quad (16)$$

while in the regions 3 and 4, with no obstacle present, the basis functions are equal to each other and given by

$$\psi_n^{(3)}(\rho, \varphi) = \psi_n^{(4)}(\rho, \varphi) \sqrt{\frac{2 - \delta_{n,0}}{\pi(R_W - R_C)}} \cos\left(\frac{n\pi\rho}{(R_W - R_C)}\right) \cos\left(\frac{k}{2}\varphi\right). \quad (17)$$

Here we can use the definition of the transverse wave number γ_n , i.e., $\gamma_n^2 = \omega^2\mu\varepsilon - k_{zn}^2$, where we denote the longitudinal wave number for the n -th mode by k_{zn} . Thus, the longitudinal wave numbers $k_{zn}^{(i)}$ and the TM_n -mode impedances $Z_n^{(i)}$ for the four regions ($i = 1, 2, 3, 4$) can be written in the form

$$k_{zn}^{(i)2} = \omega^2\mu\varepsilon - \gamma_n^{(i)2}, \quad (18)$$

$$Z_n^{(i)} = \frac{k_{zn}^{(i)}}{k} \eta, \quad \eta = \sqrt{\frac{\mu}{\varepsilon}}. \quad (19)$$

The radial electric fields $E_{rn}^{(i)}$ and azimuthal magnetic fields $H_{\varphi n}^{(i)}$ are now linear combinations of the basis functions $\psi_n^{(i)}(\rho)$ for the respective

region. These transverse fields can be expanded, in terms of the basis functions, as follows [9]:

$$E_r^{(i)}(\rho, \varphi, z) = \sum_{n=0}^{\infty} \left[c_n^{(i)+}(z) + c_n^{(i)-}(z) \right] Z_n^{(i)} \psi_n^{(i)}(\rho, \varphi), \quad (20)$$

$$H_\varphi^{(i)}(\rho, \varphi, z) = \sum_{n=0}^{\infty} \left[c_n^{(i)+}(z) - c_n^{(i)-}(z) \right] \psi_n^{(i)}(\rho, \varphi). \quad (21)$$

where for each mode and each region $E_{rn}^{(i)} = Z_n^{(i)} H_{\varphi n}^{(i)}$, while $c_n^{(i)\pm}(z)$ are coefficients for modes propagating in $\pm z$ -direction. Here we need to consider the boundary conditions at the planes $z = z_1$ and $z = z_2$. First, we have the continuity of the transverse electric field component E_r over the entire surface, where $\mathbf{E} = \mathbf{0}$ inside the conductive material yields that E_r vanishes at the metallic part of the boundary. The second condition is that H_φ must be continuous over the aperture parts of the surface. In Equations (20) and (21), the sum is performed over all modes ($0 \leq n \leq \infty$), but in the numerical implementation, each summation needs to be reduced from ∞ to a maximum mode number N_i ($i = 1, 2, 3, 4$). Thus, with a finite number of modes ($0 \leq n_i \leq N_i$), we define the vectors $\mathbf{c}_{(i)}^\pm(z)$ by ($i = 1, 2, 3, 4$)

$$\mathbf{c}_{(i)}^\pm(z) = \left[c_1^{(i)\pm}(z) \quad c_2^{(i)\pm}(z) \quad \dots \quad c_{N_i}^{(i)\pm}(z) \right]^T. \quad (22)$$

Following [5], the scattering analysis gives the following results

$$\begin{bmatrix} \mathbf{c}^-(z_L) \\ \mathbf{c}^+(z_R) \end{bmatrix} = \begin{bmatrix} \mathbf{S}_{11} & \mathbf{S}_{12} \\ \mathbf{S}_{21} & \mathbf{S}_{22} \end{bmatrix} \begin{bmatrix} \mathbf{c}^+(z_L) \\ \mathbf{c}^-(z_R) \end{bmatrix}. \quad (23)$$

Thus we obtain the complete scattering matrix equation for propagation over one ‘‘cell’’, i.e., from z_L to z_R . The cascading of one cell denoted by a , with scattering matrix \mathbf{S}^a and situated in the interval $z_1 \leq z \leq z_2$, with a neighboring cell denoted by b , with scattering matrix \mathbf{S}^b and situated in the interval $z_2 \leq z \leq z_3$, gives the following scattering equation:

$$\begin{bmatrix} \mathbf{c}^-(z_1) \\ \mathbf{c}^+(z_3) \end{bmatrix} = \begin{bmatrix} \mathbf{S}_{11}^c & \mathbf{S}_{12}^c \\ \mathbf{S}_{21}^c & \mathbf{S}_{22}^c \end{bmatrix} \begin{bmatrix} \mathbf{c}^+(z_1) \\ \mathbf{c}^-(z_3) \end{bmatrix}, \quad (24)$$

where the cascading formulae for the elements of the total scattering matrix \mathbf{S}^c can be found in e.g., [14]. Using the total cascading formula (24), it is possible to cascade together any number of cells by iteration.

5. RESULTS AND DISCUSSION

The computer simulation geometry of our transformer winding model is shown in Fig. 4. At this stage, we are mainly concerned with investigating the diagnostic principles, such that the dimensions chosen in Fig. 4 are not intended to mimic a realistic power transformer. It should be noted that the reconstruction of elliptic or wave-shaped deformations here corresponds to the reconstruction of the equivalent effective radial extensions [6], as shown in Fig. 4. The inverse problem to determine the studied parameters $\mathbf{x} = (\rho_1, \rho_2, \dots, \rho_n)$ is based on minimizing the optimization function J , defined by

$$J(\mathbf{x}) = \sum_{i,j} \left| S_{ij}^{\text{calc}}(\mathbf{x}) - S_{ij}^{\text{meas}} \right|^2, \tag{25}$$

where $S_{ij}^{\text{calc}}(\mathbf{x})$ are the elements of the calculated scattering matrix, and S_{ij}^{meas} are the corresponding elements of the measured scattering matrix. In the present paper, the studied parameters are the radial positions of the winding turns that reflect the mechanical deformations according to the formulae (12). The optimization model is tested by comparing our calculated scattering data with synthetic measurement data from a full-wave simulation performed with the commercial FEM program Ansoft HFSS. Here we present a case of reconstruction of 10 conductors, where two of the conductors are subject to wave-shaped

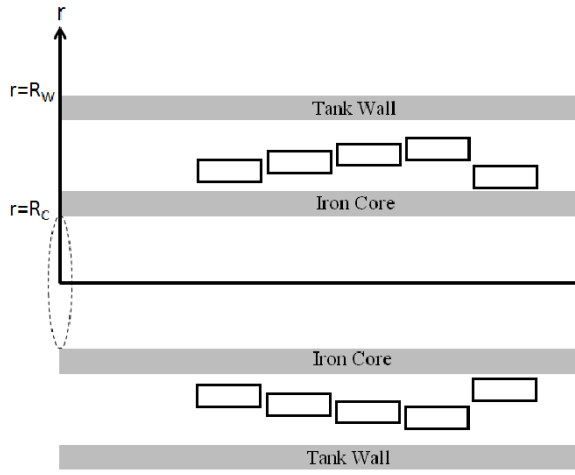


Figure 4. The problem geometry with a distance between the tank wall and iron core $R_W - R_C = 1$ m and five winding turns, each of width $R'_2 - R'_1 = 0.3$ m and height $z_2 - z_1 = 0.9$ m.

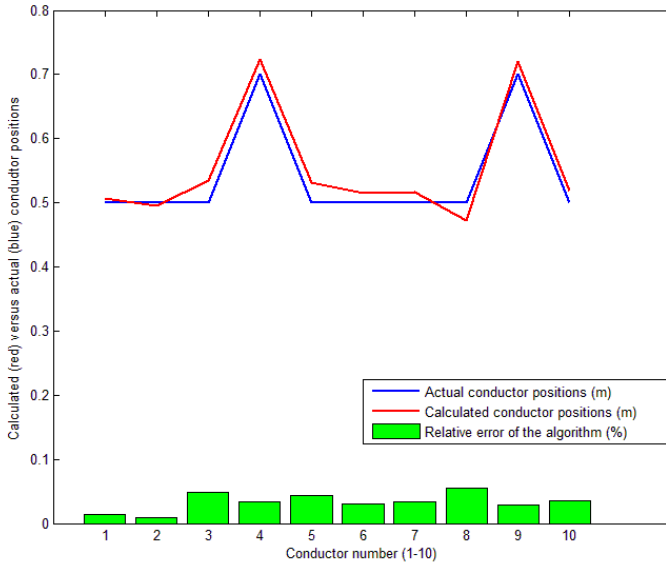


Figure 5. Calculated (red line) versus actual (blue line) conductor positions, for the case of ten conductor cells at $f = 250$ MHz.

deformations. The results are shown in Fig. 5, where we obtained good reconstruction results for the effective winding positions that reflect the corresponding mechanical deformations according to the formulae (12).

6. CONCLUSION

We studied general wave-shaped deformations of winding turns in a power transformer using first-order perturbation theory. We simulated antennas inside the transformer tank to radiate and measure microwave fields in order to identify and quantify wave-shaped deformations of winding segments or individual turns. Using optimization to solve the inverse problem, we obtained a good agreement between the reconstructed and true deformations of the winding turns.

It should however be noted that in the present stage, we are mainly concerned with investigating the potential diagnostic principles, so one can generally say that our present numerical investigations are for “training” purposes. A proper testing of the actual accuracy of the proposed model will be possible when we run a model of an actual transformer with realistic dimensions, with actual measurement data and when we further improve our optimization algorithm. Such an investigation will be the subject of further studies.

ACKNOWLEDGMENT

This work was funded by the Swedish Energy Agency, Project Nr. 34146-1.

REFERENCES

1. Mackenzie, E. A., J. Crossey, A. de Pablo, and W. Ferguson, "On-line monitoring and diagnostics for power transformers," *Conference Record of the 2010 IEEE International Symposium on Electrical Insulation (ISEI)*, 1–5, San Diego, CA, June 6–9, 2010.
2. Vaessen, P. T. M. and E. Hanique, "A new frequency response analysis method for power transformers," *IEEE Transactions on Power Delivery*, Vol. 7, No. 1, 384–391, January 1992.
3. Shao, Y., Z. Rao, and Z. Jin, "Online state diagnosis of transformer windings based on time-frequency analysis," *WSEAS Transactions on Circuits and Systems*, Vol. 8, No. 2, 227–236, February 2009.
4. Abeywickrama, N., Y. V. Serdyuk, and S. M. Gubanski, "High-frequency modeling of power transformers for use in frequency response analysis (FRA)," *IEEE Transactions on Power Delivery*, Vol. 23, No. 4, 2042–2049, 2008.
5. Dalarsson, M., A. Motevasselian, and M. Norgren, "On using multiple modes to reconstruct conductor locations in a power transformer winding," *PIERS Proceedings*, 516–523, Kuala Lumpur, Malaysia, March 27–30, 2012.
6. Dalarsson, M., A. Motevasselian, and M. Norgren, "Using multiple modes to reconstruct conductor locations in a cylindrical model of a power transformer winding," *International Journal of Applied Electromagnetics and Mechanics*, Vol. 41, No. 3, 279–291, 2013.
7. Myska, R. and P. Drexler, "Simulation and verification of methods for partial discharge source localization," *PIERS Proceedings*, 704–708, Kuala Lumpur, Malaysia, March 27–30, 2012.
8. Colton, D. and R. Kress, *Inverse Acoustic and Electromagnetic Scattering Theory*, Springer, Berlin, 1992.
9. Masterman, P. H. and P. J. B. Clarricoats, "Computer field-matching solution of waveguide transverse discontinuities," *Proc. IEEE*, Vol. 118, 51–63, 1971.
10. Jackson, J. D., *Classical Electrodynamics*, 3rd Edition, Wiley, New York, 1999.
11. Schelkunoff, S. A., *Electromagnetic Waves*, D. Van Nostrand Company, Inc., New York, 1943.

12. ABB, *Transformer Handbook*, 2004.
13. Li, Y., G. Liu, L. Zhang, L. Zhang, and Z. Lin, "Transformer winding deformation diagnosis using middle band frequency response analysis," *2007 International Conference on Solid Dielectrics*, 677–680, Winchester, UK, July 8–13, 2007.
14. Omar, A. and K. Schonemann, "Transmission matrix representation of finline discontinuities," *IEEE Transactions on Microwave Theory and Techniques*, Vol. 33, 765–770, 1985.